Research Article

Fatemah H. Alkallas, Amira Ben Gouider Trabelsi, Asmaa M. Elsayed*, and Mohamed Rabia*

Development of a photoelectrode based on a bismuth(III) oxyiodide/intercalated iodide-poly (1*H*-pyrrole) rough spherical nanocomposite for green hydrogen generation

https://doi.org/10.1515/phys-2025-0167
received January 25, 2025; accepted May 02, 2025

Abstract: This study presents the innovative design and development of a bismuth(III) oxyiodide/intercalated iodide-poly(1*H*-pyrrole) rough spherical nanocomposite (Bi(III)OI/I-P1HP RS-nanocomposite) as a next-generation photocathode for sustainable hydrogen production directly from seawater. The material features a unique rough-surfaced spherical morphology, composed of finely distributed nanoparticles averaging 15 nm in diameter, which enhances the surface area and light interaction. The strategic incorporation of iodide components significantly boosts photon absorption, while the optimal bandgap of 2.45 eV enables efficient light harvesting from the ultraviolet to mid-visible spectral range – ideal for real-world solar-driven applications. Hydrogen evolution experiments conducted using both natural Red Sea seawater and a synthetically formulated laboratory electrolyte demonstrated consistent and efficient performance, with current densities (J_{ph}) in light of −0.20 and −0.19 mA cm^{-2}, respectively. These values correspond to an impressive hydrogen production rate of 5.0 μmol h^{-1} cm^{-2}. The photocathode exhibited remarkable operational stability and reproducibility under chopped illumination, confirming its robustness under dynamic light conditions. Furthermore, spectral response studies across various wavelengths revealed adaptable behavior based on photon energy, underscoring its versatility in different lighting environments. With its compelling combination of high photoelectrochemical efficiency, structural stability, and economic viability, the Bi(III) OI/I-P1HP RS-nanocomposite emerges as a promising candidate for scalable, eco-friendly hydrogen generation. This work lays the foundation for future industrial applications in renewable energy, offering a practical and sustainable route toward clean fuel production directly from seawater.

Keywords: bismuth(III) oxyiodide, intercalated iodide, poly (1*H*-pyrrole), spherical nanocomposite, hydrogen generation

1 Introduction

Hydrogen (H_2) generation as a clean energy source [1,2] estimates the development of primary resources needed for producing clean H_2 fuel. However, a major challenge persists in controlling production costs, which limits the utilization of hydrogen as a viable energy alternative [1,3]. This challenge has driven extensive investigations into new materials and innovative techniques to enhance both stability and cost-effectiveness in hydrogen fuel production. One of the most fundamental methods for generating H_2 gas is water splitting, a process that breaks down water molecules through a photocatalytic reaction [4,5]. Photocatalysis plays a critical role in this process, converting light energy into chemical energy to facilitate this reaction. A variety of semiconducting materials: sulfides, nitrides, and organic compounds, besides the oxides, have been utilized as photocatalysts for hydrogen production. Among these, metal oxides stand out due to their cost-effectiveness and the relative simplicity of their preparation, making them highly suitable for large-scale hydrogen generation [2,6,7]. Other materials possess the capability to facilitate heat transfer through interfacial connections, making them suitable for use in various energy systems [8–10]. Metal oxides and plasmonic materials, in particular, demonstrate potential for applications in thermal energy

* **Corresponding author: Asmaa M. Elsayed**, TH-PPM Group, Physics Department, Faculty of Science, Beni-Suef University, Beni-Suef, 62514, Egypt, e-mail: asmaa.elsayed@science.bsu.edu.eg
* **Corresponding author: Mohamed Rabia**, Nanomaterials Science Research Laboratory, Chemistry Department, Faculty of Science, Beni-Suef University, Beni-Suef, 62514, Egypt, e-mail: mohamedchem@science.bsu.edu.eg
Fatemah H. Alkallas, Amira Ben Gouider Trabelsi: Department of Physics, College of Science, Princess Nourah bint Abdulrahman University, P.O. Box 84428, Riyadh, 11671, Saudi Arabia

transfer as well as in energy-related biological evaluations [11–15]. To improve the efficiency of photocatalysts, several strategies have been developed. Enhancing the surface area of the material is a common approach, as it provides more active sites under modifications to enhance the ability of the material to capture and utilize light energy, leading to improved hydrogen gas production. Such advancements demonstrate the importance of optimizing photocatalyst properties to achieve more efficient and sustainable hydrogen generation [16,17].

Bismuth materials are promising candidates for hydrogen production through water splitting. These materials, which fall under the category of chalcogenides, have seen extensive use in recent years. Bismuth-based semiconductors encompass a wide range of materials, such as Bi_2MoO_6/TiO_2, $BiWO_6$, $Bi_2WO_6/BiVO_4$, Bi_2O_3/Bi_2WO_6, $ZnIn_2S_4/BiVO_4$, and Bi_2O_3/Bi_2WO_6. These materials are well-suited for photocatalytic applications [18,19]. For instance, bismuth oxyhalides, such as bismuth oxyiodide (BiOI) and bismuth oxychloride (BiOCl), have demonstrated exceptional catalytic efficiency in water splitting. This high efficiency can be attributed to their smaller bandgap, which allows them to absorb a broader spectrum of light, thereby enhancing their photocatalytic activity.

The optical properties of bismuth-based materials are particularly advantageous for photocatalysis. Their ability to effectively capture and utilize light energy accelerates the water-splitting process, leading to faster hydrogen generation. Additionally, bismuth-based heterostructures have shown remarkable electrocatalytic performance, benefiting from a strong synergistic effect between their components. These heterostructures provide enhanced charge separation and transfer, further improving the efficiency of hydrogen production [20].

Given the versatility of bismuth materials, there is significant potential for designing and synthesizing novel bismuth-based compounds with even higher hydrogen generation capabilities. By exploring various combinations and configurations of bismuth compounds, researchers can develop materials with tailored properties to meet the specific demands of hydrogen production. This opens up new possibilities for achieving more efficient and sustainable hydrogen generation, contributing to the global transition toward renewable energy sources. Hydrogen production offers a promising solution to the global energy crisis while reducing dependence on fossil fuels. As advancements in this field continue, the development of low-cost hydrogen gas technologies is expected to be instrumental in achieving a sustainable energy future. Moreover, the use of unconventional electrolytes presents a significant challenge that, if addressed, could make hydrogen generation more feasible and widely adopted [21–24].

In this study, we present the design and development of a novel nanoporous Bi(III)OI/I-P1HP RS-nanocomposite photocathode for sustainable hydrogen production, utilizing seawater as a natural and abundant electrolyte. The strategic incorporation of iodide-based components, confirmed through X-ray photoelectron spectroscopy (XPS) and X-ray diffraction (XRD), significantly enhances the material's light-harvesting capabilities. Comprehensive optical and structural analyses were conducted using both Red Sea seawater and an artificial electrolyte to evaluate hydrogen evolution performance. The system demonstrated remarkable stability and efficiency under chopped light conditions and across a broad range of wavelengths. These findings underscore the photocathode's strong potential as a scalable, cost-effective solution for green hydrogen generation, offering a valuable contribution to next-generation renewable energy technologies.

2 Experimental section

2.1 Materials and devices

Ethanol (99.9%) and pyrrole (9.9%) were sourced from Acros, USA. HCl (37%) was procured from VWR, Germany. Acetic acid (99.9%), potassium iodide (99.8%), bismuth nitrate (Bi$(NO_3)_3$) (99.9%), $(NH_4)_2S_2O_8$ (99.9%), and iodine (99.9%) were supplied by Pio-Chem, Egypt.

The 3D morphology was examined using scanning electron microscopy (SEM, Zeiss) and transmission electron microscopy (TEM, JEOL) analyses. Chemical structure characterization involved XRD (X'Pert), XPS (Kratos), and Fourier transform infrared (FTIR) spectroscopy (Bruker) analyses, while optical properties were analyzed with a PerkinElmer spectrometer.

2.2 Fabrication of the Bi(III)OI/I-P1HP RS-nanocomposite thin-film photocathode

The Bi(III)OI/I-P1HP RS-nanocomposite photocathode was fabricated as a thin film using a two-step method. Initially, 1*H*-pyrrole was polymerized in an I_2/KI solution, maintaining a monomer-to-iodide ratio of 1:3 and a monomer concentration of 0.06 M. The monomer was dissolved in 5 mL of 1 M acetic acid to ensure a homogeneous solution. A clean glass slide was put inside the flask during polymerization, allowing the P1HP-I complex to form and deposit onto the slide at 25°C. In the second step, 0.05 M Bi

$(NO_3)_3$ was introduced into the polymer-coated film to synthesize the Bi(III)OI/P1HP RS-nanocomposite, yielding a promising photocathode. The final treatment involved soaking the film in distilled water for 5 min and then drying for 1 h at a warm temperature.

For the pristine P1HP polymer, a similar polymerization process was followed, using $(NH_4)_2S_2O_8$ as the oxidizing agent instead of I_2/KI while keeping the monomer-to-oxidant ratio consistent. HCl replaces acetic acid as the solvent, both maintained at 1 M. Under these conditions, a uniform P1HP film was deposited onto a glass substrate. This fabrication approach produced high-quality thin films suitable for efficient photocathode applications in sustainable energy systems.

2.3 Conversion of seawater into H_2 gas using the Bi(III)OI/I-P1HP RS-nanocomposite thin film photocathode

The conversion of seawater into hydrogen gas was carried out using the photoelectrochemical technique, employing the fabricated Bi(III)OI/I-P1HP RS-nanocomposite thin-film photocathode. A three-electrode cell was assembled for this process, with the photocathode served as the working electrode to drive the reduction reaction. Seawater from the Red Sea (collected near Hurghada city) was used as the electrolyte. This seawater contains ions that act as efficient sacrificial agents, facilitating water movement and enhancing the splitting reaction. During the process, H_2 gas

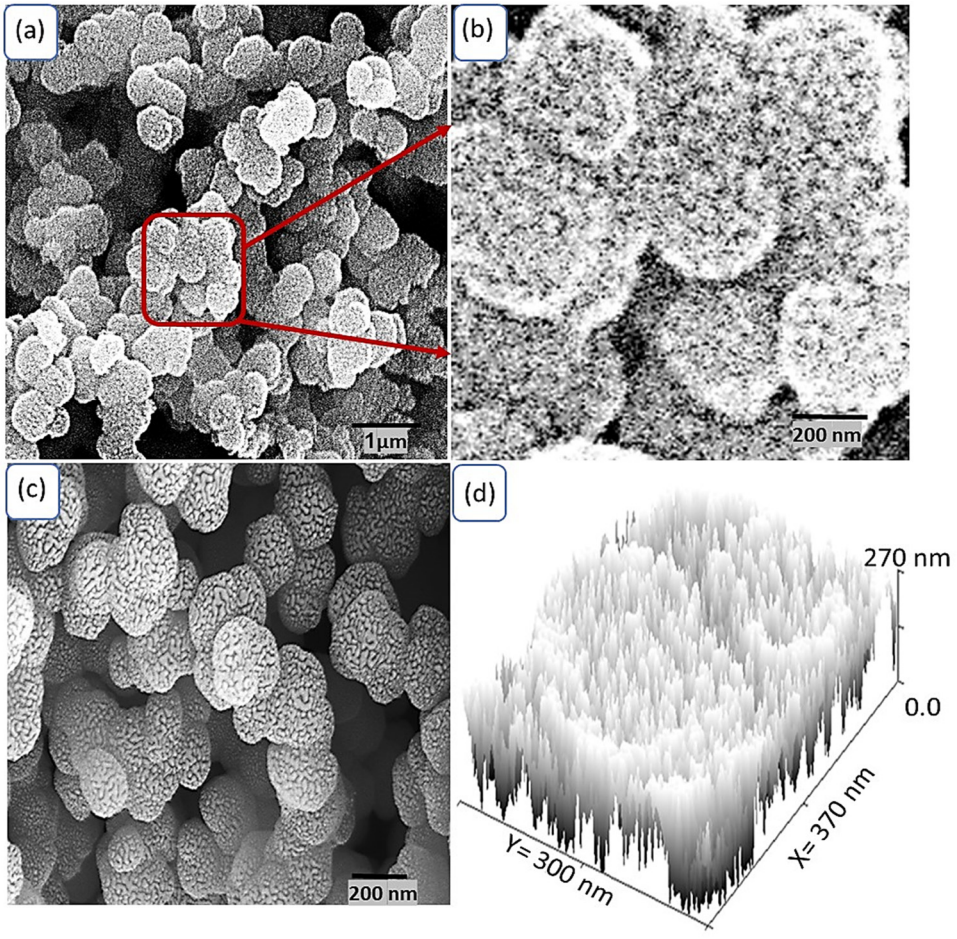

Figure 1: Morphology of the Bi(III)OI/I-P1HP RS-nanocomposite: (a) and (b) SEM images at different scales and (d) cross-section modeling image. (c) SEM image of pristine P1HP.

evolved at the cathode, while chlorine gas was released at the counter electrode, which was made of graphite. The reaction was regulated through precise alignment of potential with a reference calomel electrode.

To further understand the role of ions present in natural seawater, a secondary electrolyte was used, consisting of laboratory-synthesized artificial seawater. This artificial seawater mimics the composition of Red Sea water and includes Na_2SO_4, $MgCl_2$, $KHCO_3$, NaCl, and $CaCl_2$ at concentrations of 5.26, 19.06, 0.24, 38.38, and 2.43 g L^{-1}, respectively [17]. By comparing natural and artificial seawater, the contribution of individual ions to the splitting reaction and H_2 gas evolution can be analyzed.

Electrochemical measurements were conducted using a CHI workstation, which records key parameters such as the applied potential and current density. The device also monitors current density variations over time under chopped light illumination. The amount of H_2 gas produced was calculated from the measured current density using Faraday's law (Eq. (1)) [23]. By determining the current density (J_{ph}), the photocathode's efficiency in generating H_2 gas was assessed, along with the comparative performance of natural and artificial seawater in facilitating the splitting reaction.

The photocathode's catalytic performance was evaluated under various illumination conditions, including single-wavelength light sources, white light, and complete darkness. This approach enables the determination of the photocathode's photocatalytic efficiency in diverse lighting scenarios. The photocathode's ability to respond to different wavelengths is particularly significant for understanding its potential in real-world applications where light availability may vary. Overall, the Bi(III)OI/I-P1HP RS-nanocomposite thin-film photocathode demonstrates promising potential in driving the photoelectrochemical conversion of seawater into H_2 gas. The study highlights the role of seawater ions in enhancing the reaction, as well as the utility of artificial seawater for controlled experiments. These findings provide sustainable hydrogen production technologies.

$$H_2\text{mole} = \int_0^t J_{ph} \cdot dt/F. \quad (1)$$

3 Results and discussion

3.1 Physicochemical characteristics

The surface morphology of the Bi(III)OI/I-P1HP RS-nanocomposite was examined using SEM, as depicted in Figure 1(a) and (b). The images display spherical particles with diameters ranging from approximately 200 to 500 nm, featuring notably rough surfaces. This roughness results from the dispersion of smaller nanoparticles, averaging around 10 nm, across the larger spheres. These nanoscale structures notably enhance the active surface area, thereby increasing the number of reactive sites available for the water-splitting reaction and improving the hydrogen production efficiency.

The cross-sectional model shown in Figure 1(d) provides important information about the internal architecture of the nanocomposite. The analysis reveals a uniform distribution of P1HP and Bi(III)OI components, marked by porous, evenly dispersed spherical nanoparticles (~15 nm) layered over larger spherical structures. These fine particles are crucial for improving light absorption and photon capture, which significantly enhances the photocatalytic performance of the material [25,26]. This optimized photon interaction contributes to the nanocomposite's improved efficiency in generating hydrogen gas under light exposure.

For comparison, the pristine P1HP polymer was also characterized through SEM, as shown in Figure 1(c). The SEM images of P1HP reveal that the formation of spherical particles is a defining characteristic of this polymer. This morphology reflects the high efficiency of the polymerization process, resulting in a material with unique structural properties. The observed spherical shape not only supports excellent polymerization but also explains the suitability of the P1HP polymer as a matrix for incorporating the Bi(III)OI inorganic component.

The distinctive structural features of the Bi(III)OI/P1HP RS-nanocomposite, such as the rough surface and the presence of small coating particles, justify its superior performance in photoelectrochemical applications. The incorporation of Bi(III)OI into the P1HP matrix enhances the material's functionality by leveraging the complementary properties of both components. The P1HP polymer provides a robust framework with excellent polymerization characteristics, while the Bi(III)OI material contributes to light absorption and catalytic activity. Together, these attributes create a synergistic effect that enhances the nanocomposite's overall performance, particularly for H_2 gas production.

So, the structural analysis of the Bi(III)OI/I-P1HP RS-nanocomposite demonstrates its promising potential for photoelectrochemical applications. The rough surfaces, nanoscale features, and homogeneous material integration collectively contribute to its ability to efficiently capture photons and facilitate splitting reactions.

The chemical structure of the Bi(III)OI/I-P1HP RS-nanocomposite was analyzed by evaluating its functional groups using FTIR (Figure 2(a)) and Table 1; the functional

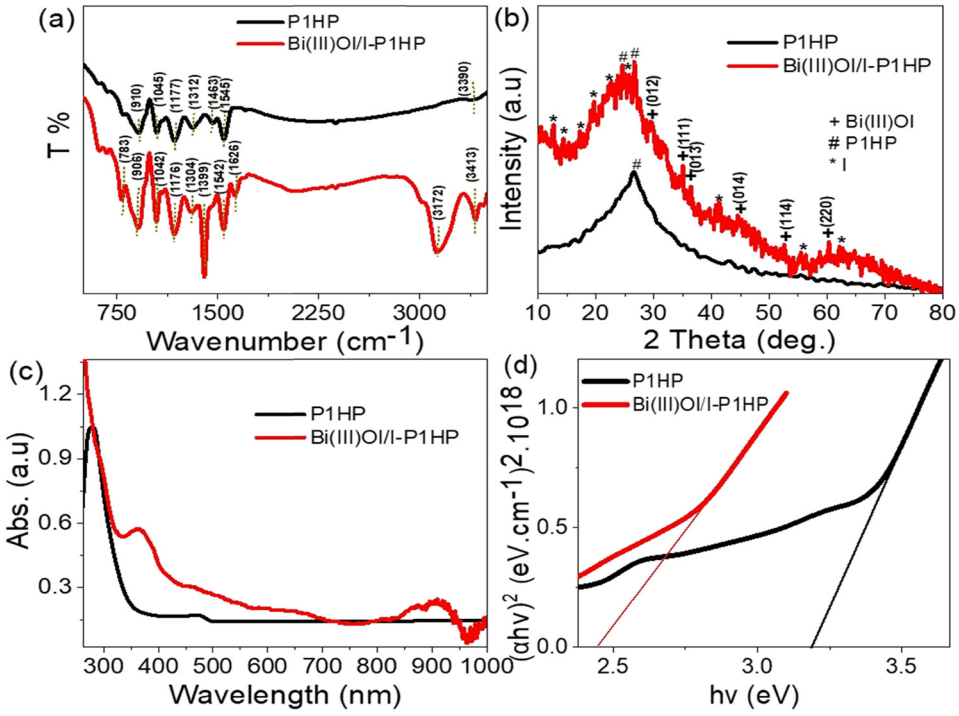

Figure 2: (a) FTIR analysis, (b) XRD analysis of the crystalline structure, and (c) and (d) optical absorption and bandgap evaluation, respectively, of the synthesized Bi(III)OI/I-P1HP RS nanocomposite in comparison to pure P1HP.

groups in the composite are compared to those in the pure P1HP polymer. The FTIR analysis revealed noticeable shifts in the characteristic absorption bands of the composite relative to the pure P1HP polymer, confirming the successful incorporation of Bi(III)OI and iodide structures into the polymer matrix [27,28]. For instance, the distinct vibrational bands of the P1HP ring, originally observed at 1,545 and 1,626 cm^{-1} in the pure polymer, were shifted to 1,542 cm^{-1} in the composite. Additionally, the C–N stretching vibration, which appeared at 1,312 cm^{-1} in the pristine polymer, shifted to 1,304 cm^{-1} in the composite [29]. These quantitative shifts indicate successful structural integration within the nanocomposite. This integration introduces modifications into the internal structure of the composite, influencing its overall chemical and physical properties. The shifts are indicative of interactions between the inorganic Bi(III)OI and iodide species with the polymer, which leads to alterations in the polymer's chemical environment and results in synergistic effects that enhance the material's optical behavior.

This modification of the polymer structure affects its optical properties with significant impact on the composite's electrical behavior. The incorporation of the inorganic Bi(III)OI and iodide into the polymer network introduces additional interactions that modify the charge transfer and conductivity characteristics, making the composite more suitable for great applications: photocatalysis or energy conversion processes. Moreover, this provides a crystal material with structural stability and performance. The presence of Bi(III)OI and iodide could lead to the formation of new crystalline phases or enhance the existing crystalline structure of the polymer, thereby improving the composite's mechanical strength and durability. This structural enhancement is likely to improve the efficiency of the composite in various applications, particularly in conversion processes such as hydrogen production, where both the optical and electrical properties are critical.

Table 1: FTIR bands for the Bi(III)OI/I-P1HP RS-nanocomposite relative to the P1HP pure polymer

Bond positions (cm^{-1})		Functional groups
P1HP	**Bi(III)OI/I-P1HP RS-nanocomposite**	
1,545	1,626 and 1,542	P1HP ring [30]
1,463	1,399	C–C [29]
1,045 and 1,177	1,042 and 1,176	C–H
1,312	1,304	C–N
910	783 and 906	Disubstituted sites

The crystalline structure of the Bi(III)OI/I-P1HP RS-nanocomposite was analyzed to assess the improvements made upon incorporating the inorganic Bi(III)OI and iodide components, relative to the pure P1HP polymer. As illustrated in Figure 2(b), the composite exhibits six distinct peaks corresponding to Bi(III)OI, nine weaker peaks for iodide, and two sharp peaks for the P1HP polymer within the composite structure. These six Bi(III)OI peaks are observed at 29.6°, 35.2°, 36.6°, 44.8°, 52.7°, and 60.6°, which correspond to the Miller index growth directions (012), (111), (013), (104), (114), and (220), respectively [31]. In contrast, the P1HP polymer within the composite is represented by two sharp peaks at 24.7° and 26.9°.

When compared to the pure P1HP polymer, which displays a single semi-sharp peak at 24.4°, the Bi(III)OI/I-P1HP composite demonstrates significant changes in its crystalline structure. The additional peaks' appearance and the sharper nature of the P1HP polymer peaks suggest an improvement in the overall crystallinity of the composite. The single semi-sharp peak in the pure P1HP polymer reflects its semi-crystalline nature, but the incorporation of Bi(III)OI and iodide materials leads to a more organized and well-defined crystalline structure in the composite. This modification enhances the material's overall photon absorption properties under light illumination, making it more efficient in absorbing light and facilitating energy conversion processes.

The crystalline nature of the composite is related to the presence of Bi(III)OI and iodide, which also contributed to the material's enhanced structural stability, vital for its performance in various applications. The increased crystallinity suggests a more ordered arrangement of molecules, which in turn can lead to improved charge transport, higher mechanical strength, and greater stability under operating conditions.

To further quantify the enhancement in the crystalline properties, the crystallite size was estimated using Eq. (2) [32,33] with an evaluated crystallite size of 14 nm for the Bi(III)OI/I-P1HP RS-nanocomposite. This relatively small crystallite size indicates a high surface area causing great photon absorption and energy conversion. The small crystallites also contribute to better light absorption efficiency, which is essential for photocatalytic processes or energy harvesting applications.

The overall crystalline structure, combined with improved photon absorption, makes the synthesized Bi(III)OI/I-P1HP RS-nanocomposite highly suitable for energy conversion applications. The presence of Bi(III)OI and iodide materials within the composite contributes not only to the enhancement of the crystalline nature but also to its optical and electrical properties. The ability of the composite to absorb light more effectively and convert it into useful energy makes it a promising candidate for energy-related processes.

The optical behavior of the Bi(III)OI/I-P1HP RS nanocomposite was assessed by monitoring its absorbance across different optical regions, as illustrated in Figure 2(c). The composite demonstrates significant absorbance in the UV–visible regions, extending beyond 500 nm. This highlights the composite's capability to effectively utilize photons within these regions, facilitating enhanced photon trapping and capturing. This ability to absorb photons provides additional kinetic energy to the electrons. These energized electrons undergo transitions and accumulate in the conduction band of the composite structure.

The enhanced optical absorbance observed in the iodide-based materials is a key factor in promoting photon absorption. This characteristic drives the excitation of electrons to higher energy states, enabling transitions to the conduction band. The superior photon-trapping efficiency of the composite ensures that more photons are absorbed, leading to the generation of a greater number of hot electrons. This, in turn, enhances the material's optical performance and makes it highly suitable for applications involving light-driven processes.

This behavior is further reflected in the estimated bandgap of the Bi(III)OI/I-P1HP RS nanocomposite, estimated to be 2.45 eV, as shown in Figure 2(d). The bandgap estimation is based on Eq. (3) [34,35], which utilizes the absorption coefficient as a critical parameter. The reduced bandgap indicates that the composite requires lower energy photons for electronic excitation, thereby broadening its absorption spectrum and increasing its efficiency in utilizing light energy.

In contrast, pure P1HP exhibits less favorable optical performance. Its photon absorbance is comparatively lower, which directly impacts its optical behavior and efficiency. As a result, pure P1HP has a larger bandgap of 3.2 eV, requiring higher energy photons for excitation and limiting its effectiveness in applications involving photon-driven processes.

$$D = 0.9\lambda/\beta\cos\theta, \tag{2}$$

$$\alpha h\nu = A(h\nu - E_g)^{1/2}. \tag{3}$$

The oxidation states and elemental composition of the Bi(III)OI/I-P1HP RS-nanocomposite were analyzed using XPS. This analysis provides valuable insights into the oxidation state of the central Bi element and its bonding characteristics, as well as the role of iodide within the composite structure. The XPS data help to elucidate the interactions between Bi(III)OI and the P1HP polymer, which

are critical for understanding the material's overall properties. Figure 3(a) shows the elemental composition of the nanocomposite, revealing the presence of iodine (I), oxygen (O), nitrogen (N), carbon (C), and bismuth (Bi). These elements correspond to the components used in the preparation of the composite, including the oxidant. For the P1HP polymer, the nitrogen (N) and carbon (C) elements are detected at 400 and 285.8 eV, respectively, for the 1s transition. These peaks are consistent with the elemental composition of the P1HP polymer, reflecting that the polymer remains intact during the composite reaction.

The XPS analysis for the Bi element, shown in Figure 3(b), reveals two prominent peaks for the Bi $4f_{7/2}$ and Bi $4f_{5/2}$ orbitals at 158.5 and 163.8 eV, respectively [36]. These values are indicative of bismuth in the +3 oxidation state, confirming the presence of Bi(III) in the composite. Additionally, the interaction between Bi(III) and oxygen is supported by the O 1s peak at 531.6 eV in Figure 3(d), which corresponds to the formation of Bi(III)OI and verifies the successful reaction of both bismuth and oxygen into the nanocomposite. The presence of iodide is also confirmed through XPS analysis, with a distinct doublet observed at I $3d_{5/2}$ binding energies of 618.6 and 620.3 eV. These peaks reflect iodide species within the Bi(III)OI framework as well as iodide ions interacting with the P1HP polymer. The detailed spectral data provide strong evidence that iodide is not only embedded within the Bi(III)OI lattice but also forms interactions with the polymer, affirming the successful synthesis of the Bi(III)OI/I-P1HP RS-nanocomposite. XPS analysis is crucial for confirming oxidation states of the constituent materials in the Bi(III)OI/I-P1HP RS-nanocomposite. The data indicate that Bi is present as Bi(III), and iodide ions are integrated into the Bi(III)OI structure, with additional interactions with the P1HP polymer. This information provides the essential chemical structure and the interactions between the inorganic components (Bi(III)OI and iodide) and the polymer matrix, which play a great role in determining the composite's properties. These insights are crucial for understanding the material's structure–property relationships, which are essential for its potential applications in areas such as photocatalysis, energy conversion, and other technologies.

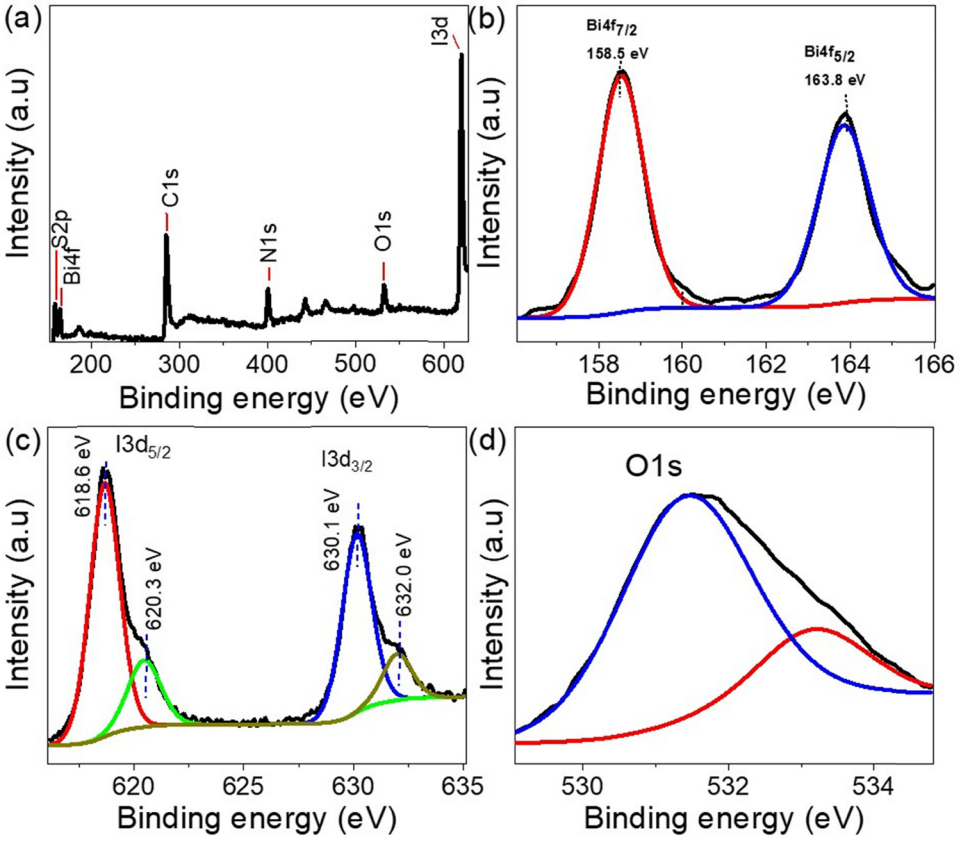

Figure 3: Elemental composition of the Bi(III)OI/I-P1HP RS-nanocomposite, as determined by XPS analysis: (a) total survey, (b) Bi, (c) I, and (d) O spectra.

3.2 Photoelectrochemical H_2 gas generation from seawater electrolyte

Photoelectrochemical hydrogen gas production represents a promising avenue for renewable energy, utilizing water sources enriched with sacrificial agents. Among these, seawater emerges as an excellent candidate, serving as a natural electrolyte abundant in ions that facilitate water splitting. These ions act as sacrificial agents, enhancing water molecule mobility under minimal applied potential. This movement propels water molecules toward the photocathode surface, where they participate in the reduction process. The availability, low cost, and eco-friendliness of seawater underscore its potential as an ideal electrolyte for hydrogen generation.

To elucidate the role of seawater ions solely as sacrificial agents – without contributing to additional reduction reactions – comparative studies are conducted. These involve employing an artificial electrolyte with a similar ionic composition to seawater, allowing a direct comparison of their respective electrochemical behaviors. All experiments utilize the CHI608E electrochemical workstation, which enables the connection of the cell and facilitates precise monitoring of changes in electrochemical reactions. These changes are evaluated by measuring the J_{ph} values, indicative of water reduction on the fabricated photocathode's surface.

The Bi(III)OI/I-P1HP photocathode demonstrates exceptional capabilities for water reduction, attributed to the unique chemical structure of its components. This photocathode consists of two semiconductors, BiOI and P1HP, which exhibit high sensitivity to incident photons. Their well-aligned energy levels synergistically enhance the charge carrier dynamics. Electrons accumulate on the BiOI surface due to its lower conduction band level relative to P1HP, while the higher valence band level of P1HP facilitates reverse hole flow. This arrangement promotes hole accumulation on the P1HP surface and efficient charge separation, critical for photoelectrochemical processes.

To assess the photocathode's performance in hydrogen gas production, J_{ph} measurements were performed using both natural and artificial seawater. Figure 4(a) illustrates that the photocurrent density under dark and light conditions is nearly identical for both electrolytes. In seawater, the current density shifts from −0.12 to −0.2 mA cm^{-2}, with similar trends observed for artificial seawater. This uniformity suggests the fabricated photocathode's robust ability to generate hydrogen from either electrolyte. Furthermore, the results confirm that seawater ions do not influence the water reduction process beyond their role as sacrificial agents.

The figure displays the transient photocurrent response of a fabricated Bi(III)OI/I-P1HP photocathode under chopped illumination, in the context of seawater splitting. The experiment was conducted under periodic light on/off cycles, which are indicated in green (on) and red (off), respectively. This behavior is characteristic of a photoelectrochemical system under intermittent light irradiation. Upon illumination ("on" period), the Bi(III)OI/I-P1HP photocathode is photoexcited, leading to electron–hole pairs. The photogenerated electrons are driven toward the external circuit due to the electric field at the semiconductor/electrolyte interface, while the holes participate in the oxidation reactions – most likely water oxidation in the context of seawater splitting. As a result, a cathodic photocurrent is observed, signifying the reduction reactions at the photocathode (*e.g.*, $H^+ + e^- \rightarrow H_2$). The negative direction of the photocurrent confirms the reduction process occurring at the photocathode side.

When turned off ("off" period), the photocurrent rapidly drops to near-zero, highlighting the absence of

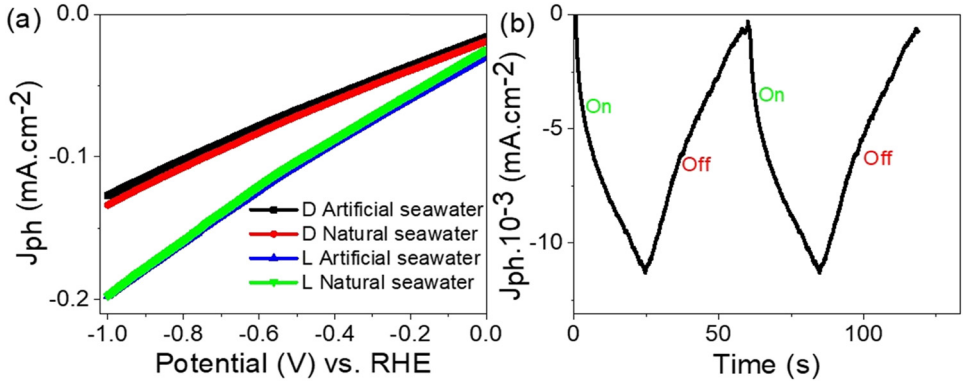

Figure 4: (a) Performance of the fabricated Bi(III)OI/I-P1HP photocathode in artificial and natural seawater electrolytes and (b) photocathode behavior under chopped light conditions.

photoexcitation and confirming that the current is photo-induced rather than due to dark reactions. The reproducibility and rapid switching response of the photocurrent across multiple cycles illustrate the excellent stability and reversibility of the Bi(III)OI/I-P1HP system under operational conditions. This behavior demonstrates the material's strong photoresponsivity, suggesting efficient charge separation and transport, minimal recombination losses, and good interaction with the seawater electrolyte. Overall, the chopped light experiment confirms that the Bi(III)OI/I-P1HP photocathode can act as a stable and efficient photoelectrode for seawater splitting, offering promising performance in terms of sustained hydrogen generation under intermittent solar illumination.

The light sensitivity of the Bi(III)OI/I-P1HP photocathode was evaluated by testing its response under various optical filters. These filters allowed the passage of monochromatic light corresponding to specific optical regions, enabling detailed analysis. In the ultraviolet (UV) region, where photons of 340 nm were transmitted, the J_{ph} was measured at −0.19 mA cm^{-2}. This value is comparable to the current density achieved under full-spectrum white light illumination (−0.2 mA cm^{-2}). This similarity is related to the high energy carried by photons in the UV region, which are associated with higher frequencies. These energetic photons interact with the active sites of the photocathode, transferring their energy to the material. This interaction activates "hot" electrons, facilitating energy transfer and enhancing the photocurrent [37,38].

As the wavelength increases, the energy and frequency of these photons decrease. Consequently, the energy transferred to the photocathode's active sites diminishes, resulting in a reduction in the generated photocurrent density. This trend is reflected in the measured J_{ph} values, which decrease to −0.18 and −0.17 mA cm^{-2} for 440 and 730 nm, respectively. Figure 5(b) provides a summary of these results, derived from the data presented in Figure 5(a), at −1.0 V.

This behavior highlights the photocathode's capability to efficiently generate hydrogen gas across different optical regions. Notably, the photocathode demonstrates superior efficiency in the UV region compared to other regions of the light spectrum. Furthermore, it confirms the photocathode's ability to sustain hydrogen generation from seawater under various optical conditions, utilizing more than 50% of sunlight effectively.

So, the Bi(III)OI/I-P1HP photocathode exhibits excellent performance in harnessing energy from different parts of the light spectrum. Its high sensitivity to UV light underscores its suitability for photoelectrochemical applications. The results also affirm the photocathode's robustness and efficiency in generating hydrogen gas from seawater under diverse optical conditions, making it viable sustainable energy solutions.

The high efficiency of the photocathode's response to various optical regions can be attributed to its unique electronic structure, as illustrated in Figure 6(a). The sequential transfer of electrons between the materials comprising the photocathode – P1HP and BiOI – is facilitated by their closely aligned conduction band energy levels. This alignment enables electrons to move effortlessly from P1HP to BiOI. As electrons accumulate on the surface of the BiOI material, they create a strong electric field, further driving electron accumulation [39,40]. This electric field supports the reduction process by facilitating interactions with adjacent seawater molecules, thereby contributing to hydrogen generation.

Simultaneously, the photogenerated holes are directed in the opposite direction, moving toward the surface of the

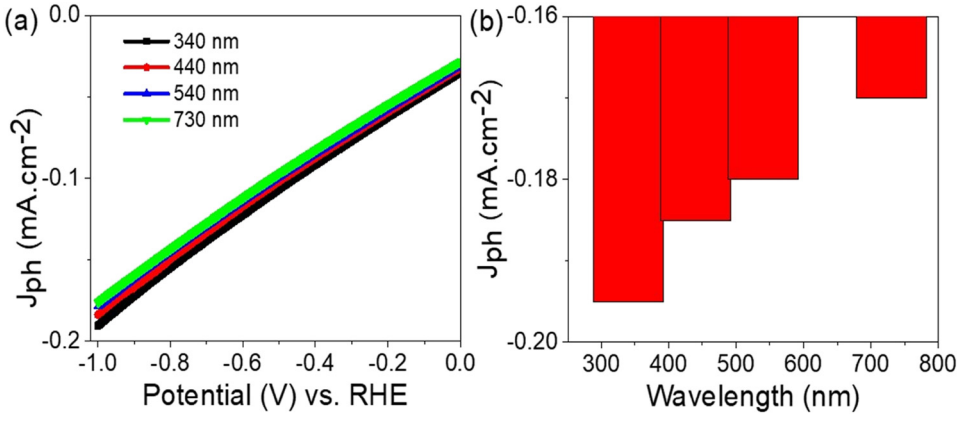

Figure 5: (a) Photocathode's response to monochromatic light, showing J_{ph} as a function of applied potential in natural seawater and (b) the calculated J_{ph} at −1.0 V.

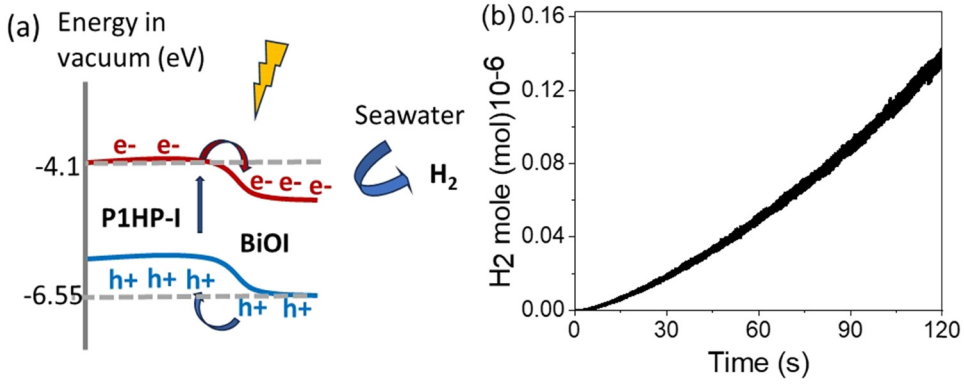

Figure 6: (a) Flow of photogenerated charge carriers through the Bi(III)OI/I-P1HP system and (b) hydrogen gas production evaluated using Faraday's equation.

P1HP material. This reverse flow of holes complements the electron transfer and establishes a closed circuit for the photogenerated charge carriers. The combined effect of polarization and the generated electric field within the photocathode system drives the reduction reaction, resulting in hydrogen gas production.

The amount of hydrogen gas generated by the photocathode has been quantified as 5.0 μmol h^{-1} cm^{-2}, as estimated in Figure 6(b). This value represents an improvement compared to other materials, such as polyaniline derivative composites with oxides or sulfides and polypyrrole composites with graphene oxide. The calculation of hydrogen production is based on Faraday's law, as expressed in Eq. (1), which relates the generated J_{ph} to the amount of hydrogen gas produced.

This promising result underscores the effectiveness of the Bi(III)OI/I-P1HP photocathode in harnessing light energy for hydrogen generation. Its superior performance compared to other materials demonstrates its potential for advancing sustainable energy applications. The ability of this photocathode to generate hydrogen efficiently, combined with its responsiveness to diverse optical regions, positions it as a leading candidate for photoelectrochemical hydrogen production technologies, in which Table 2 estimates this performance relative to other literature.

Table 2: Bi(III)OI/I-P1HP photocathode performance compared to previous studies

Photoelectrode	J_{ph} (mA cm^{-2})	Electrolyte
$BiFeO_3$ [41]	0.1	NaOH
Cr_2S_3–Cr_2O_3/poly-2-aminobenzene-1-thiol [42]	0.017	Sewage water
Poly-*m*-toluidine/graphene oxide [43]	0.09	Sewage water
Poly(3-aminobenzoic acid) [44]	0.08	H_2SO_4
TiN–TiO_2 [45]	3.0×10^{-4}	NaOH
g-C_3N_4–CuO [46]	0.01	NaOH
PrFeO [47]	0.130	Na_2SO_4
CuO–C/TiO_2 [48]	0.012	glycerol
Au/Pb(Zr, Ti)O_3 [49]	0.06	NaOH
Present work: Bi(III)OI/I-P1HP nanocomposite photocathode	0.2	Seawater

4 Conclusions

This research centers on the development of a nanoporous Bi(III)OI/I-P1HP RS-nanocomposite, engineered as a photocathode for eco-friendly hydrogen production using seawater as the working electrolyte. The strategic inclusion of iodide-based materials improves the composite's light absorption capabilities, while its moderate bandgap of 2.45 eV allows for efficient photon harvesting from UV to mid-visible regions, making it well-suited for photocatalytic processes. XPS confirmed the successful integration of iodide within both the polymeric and inorganic frameworks. XRD analysis identified nanostructures resembling cysteine with an average diameter of around 14 nm and revealed enhanced crystallinity upon embedding Bi(III)OI into the P1HP polymer. The photocathode's structural and optical attributes were investigated in the context of hydrogen evolution, achieving a hydrogen generation rate of 5.0 μmol/h cm^2. Performance evaluations were carried out using two different electrolytes: natural seawater from the Red Sea and a synthetic laboratory-prepared solution. The recorded J_{ph} were −0.20 mA cm^{-2} for Red Sea seawater and −0.19 mA cm^{-2} for the artificial medium, underscoring the system's stable and consistent performance under diverse environmental conditions. To assess operational stability, chopped illumination tests were conducted,

which demonstrated high reproducibility and excellent durability over time. Furthermore, wavelength-dependent studies revealed variable photoresponses linked to incident photon energy, indicating the material's flexibility under a broad range of light conditions. Combining strong photoconversion efficiency, long-term electrochemical stability, and cost-effectiveness, the Bi(III)OI/I-P1HP RS-nanocomposite emerges as a highly promising candidate for large-scale hydrogen production applications, contributing significantly to the advancement of renewable and sustainable energy technologies.

Acknowledgments: The authors express their gratitude to Princess Nourah bint Abdulrahman University Researchers Supporting Project number (PNURSP2025R223), Princess Nourah bint Abdulrahman University, Riyadh, Saudi Arabia.

Funding information: This research was funded by Princess Nourah bint Abdulrahman University Researchers Supporting Project number (PNURSP2025R223), Princess Nourah bint Abdulrahman University, Riyadh, Saudi Arabia.

Author contributions: Mohamed Rabia: experimental work and writing of the manuscript. Fatemah H. Alkallas: funding, supervision, and organizing the work. Amira Ben Gouider Trabelsi: writing of the manuscript, performed analysis, and organizing the work. Asmaa M. Elsayed: experimental work. All authors have accepted responsibility for the entire content of this manuscript and approved its submission.

Conflict of interest: The authors state no conflict of interest.

Data availability statement: All data generated or analyzed during this study are included in this published article.

References

[1] Liu Y, Yu C, Jiang Q, Liu Y, Fan Z, Deng H, et al. Kinetic modeling of in-situ hydrogen generation from bitumen and its influencing factors and mechanisms study. Fuel. 2025;385:134155. doi: 10.1016/J.FUEL.2024.134155.

[2] He Z, Li K, Chen T, Feng Y, Villalobos-Portillo E, Marini C, et al. High-purity hydrogen production from dehydrogenation of methylcyclohexane catalyzed by zeolite-encapsulated subnanometer platinum-iron clusters. Nat Commun. 2025;16(1):92. doi: 10.1038/s41467-024-55370-z.

[3] Uemura S, Kobayashi R, Ikegami S, Aoyama Y, Tabe Y. Electricity storage and hydrogen generation system using the electrochemical reaction of lithium and water. Int J Hydrogen Energy. 2025;100:853–62. doi: 10.1016/J.IJHYDENE.2024.12.113.

[4] Aldosari E, Rabia M, Zhang Q, Mohamed SH. High-efficiency photocathode for green hydrogen generation from sanitation water using bismuthyl chloride/poly-o-chlorobenzeneamine nanocomposite. Open Chem. 2025;23(1):20240112.

[5] Aldosari E, Rabia M, Sanna A, Farid O. Single-step fabrication of Ag_2S/poly-2- mercaptoaniline nanoribbon photocathodes for green hydrogen generation from arti fi cial and natural red-sea water. Open Phys. 2025;23(1):20240095.

[6] Chen Z, Yang M, Li Y, Gong W, Wang J, Liu T, et al. Termination-acidity tailoring of molybdenum carbides for alkaline hydrogen evolution reaction. Nat Commun. 2025;16(1):418. doi: 10.1038/s41467-025-55854-6.

[7] El-Bery HM, Abdel Naby MM, Mohamed GG, El-Khouly ME, Zakaria MB. Enhancing photocatalytic hydrogen generation on TiO_2 using thermally derived nickel-based cocatalysts from Hofmann-type cyanide coordination polymer flakes. Int J Hydrogen Energy. 2024;78:470–80. doi: 10.1016/J.IJHYDENE.2024.06.245.

[8] Algatheem AM, Taha HH, El-Sapa S. Interaction between two rigid hydrophobic spheres oscillating in an infinite Brinkman–stokes fluid. Mathematics. 2025;13(2):218. doi: 10.3390/MATH13020218.

[9] Awais M, Soomro FA, El-Sapa S, Khokhar RB. Heat transfer augmentation through engine oil-based hybrid nanofluid inside a trapezoid cavity. Mehran Univ Res J Eng Technol. 2024;43:24–33. doi: 10.22581/MUET1982.2401.2910.

[10] Awais M, Soomro FA, El-Sapa S, Khokhar RB, Almoneef AA. Comparative heat transfer analysis of nanoparticles based in nanofluids flow inside a C-shaped partially heated rectangular cavity. Mehran Univ Res J Eng Technol. 2024;43:34–44. doi: 10.22581/MUET1982.2401.2917.

[11] Ali Khan S, Yasmin S, Waqas H, Az-Zo'bi EA, Alhushaybari A, Akgül A, et al. Entropy optimized Ferro-copper/blood based nanofluid flow between double stretchable disks: Application to brain dynamic. Alex Eng J. 2023;79:296–307. doi: 10.1016/J.AEJ.2023.08.017.

[12] Muhammad K, Ahmed B, Sharaf M, Afikuzzaman M, Az-Zo'bi EA. Multiscale tribology analysis of MHD hybrid nanofluid flow over a curved stretching surface. Nanoscale Adv. 2024;6:855–66. doi: 10.1039/D3NA00688C.

[13] Malik MF, Shah SAA, Bilal M, Hussien M, Mahmood I, Akgul A, et al. New insights into the dynamics of heat and mass transfer in a hybrid (Ag-TiO_2) nanofluid using Modified Buongiorno model: A case of a rotating disk. Results Phys. 2023;53:106906. doi: 10.1016/J.RINP.2023.106906.

[14] Dhange M, Uma Devi C, Jamshed W, Eid MR, Ramesh K, Shamshuddin MD, et al. Studying the effect of various types of chemical reactions on hydrodynamic properties of dispersion and peristaltic flow of couple-stress fluid: Comprehensive examination. J Mol Liq. 2024;409:125542. doi: 10.1016/J.MOLLIQ.2024.125542.

[15] Bég OA, Espinoza DES, Kadir A, Shamshuddin M, Sohail A. Experimental study of improved rheology and lubricity of drilling fluids enhanced with nano-particles. Appl Nanosci (Switz). 2018;8:1069–90. doi: 10.1007/S13204-018-0746-4/TABLES/28.

[16] Yuan S, Zhang S, Wei J, Gao Y, Zhu Y, Wang H. Materials selection, design, and regulation of polymer-based hydrogen barrier composite coatings, membranes and films for effective hydrogen storage and transportation: A comprehensive review. Int J

Hydrogen Energy. 2024;91:555–73. doi: 10.1016/J.IJHYDENE.2024.10.066.

[17] Moradi-Alavian S, Kazempour A, Mirzaei-Saatlo M, Ashassi-Sorkhabi H, Mehrdad A, Asghari E, et al. Promotion of hydrogen evolution from seawater via poly(aniline-co-4-nitroaniline) combined with 3D nickel nanoparticles. Sci Rep. 2023;13:1–10. doi: 10.1038/s41598-023-48355-3.

[18] Wang S, Mao Z, Yu R, Li L, Kumar JM, Li X. Synthesis and characterization of Ppy/Bi_2MoO_6 heterojunction with enhanced photodegradation efficiency of Cr(VI). Opt Mater. 2023;144:114357. doi: 10.1016/J.OPTMAT.2023.114357.

[19] Feng Q, Zhou J, Zhang Y. Coupling Bi_2MoO_6 with persulfate for photocatalytic oxidation of tetracycline hydrochloride under visible light. J Mater Sci: Mater Electron. 2019;30:19108–18. doi: 10.1007/s10854-019-02266-0.

[20] Rana MM, Alam KM, Chaulagain N, Garcia J, Kumar N, Vrushabendrakumar D, et al. Tunable absorption and emission in mixed halide bismuth oxyhalides for photoelectrochemical water splitting. ACS Appl Nano Mater. 2024;7:6005–19. doi: 10.1021/ACSANM.3C05925/SUPPL_FILE/AN3C05925_SI_001.PDF.

[21] Kountouris I, Bramstoft R, Madsen T, Gea-Bermúdez J, Münster M, Keles D. A unified European hydrogen infrastructure planning to support the rapid scale-up of hydrogen production. Nat Commun. 2024;15(1):5517. doi: 10.1038/s41467-024-49867-w.

[22] Zhang Y, Guo S, Xin X, Song Y, Yang L, Wang B, et al. Plasmonic MoO_2 as co-catalyst of MoS_2 for enhanced photocatalytic hydrogen evolution. Appl Surf Sci. 2020;504:144291. doi: 10.1016/J.APSUSC.2019.144291.

[23] Rabia M, Aldosari E, Zhang Q. Green hydrogen photoelectrochemically produced from Red Sea water using a photocathode dichalcogenides (CoS_2)-CoO/Poly-2-aminothiophenol nanocomposite with moon-like shape. Chem Pap. 2024;78:5393–405. doi: 10.1007/S11696-024-03478-3/METRICS.

[24] Ali AH, Ahmed AM, Abdelhamied MM, Abdel-Khaliek AA, Abd El Khalik S, Abass SM, et al. Synthesis of lead-free Cu/$CuFeO_2$/CZTS thin film as a novel photocatalytic hydrogen generator from wastewater and solar cell applications. Opt Quantum Electron. 2024;56(5):902. doi: 10.1007/S11082-024-06375-X.

[25] He B, Zhao Z, Song L, Liu W, Yang Y, Shang J, et al. Highly efficient activation of peroxymonosulfate by the (3R + 2H)-$CuFeO_2$ nanocomposite photocatalyst: Intermediate toxicity, BVS validation ionic migration and degradation pathway. Sep Purif Technol. 2022;289:120729. doi: 10.1016/J.SEPPUR.2022.120729.

[26] Yaghoubi-berijani M, Bahramian B. Preparation and measurement of properties of BiOBr/BiOCl/PANI ternary nanocomposite for highly efficient visible light photocatalytic applications. Res Chem Intermed. 2021;47:2311–30. doi: 10.1007/S11164-021-04394-X/FIGURES/15.

[27] Naveed ur Rehman M, Munawar T, Nadeem MS, Mukhtar F, Maqbool A, Riaz M, et al. Facile synthesis and characterization of conducting polymer-metal oxide based core-shell PANI-Pr_2O–NiO–Co_3O_4 nanocomposite: As electrode material for supercapacitor. Ceram Int. 2021;47:18497–509. doi: 10.1016/J.CERAMINT.2021.03.173.

[28] Al-Muntaser AA, Alzahrani E, Abo-Dief HM, Saeed A, Alshammari EM, Al-Harthi AM, et al. Tuning the structural, optical, electrical, and dielectric properties of PVA/PVP/CMC ternary polymer blend using ZnO nanoparticles for nanodielectric and optoelectronic devices. Opt Mater. 2023;140:113901. doi: 10.1016/J.OPTMAT.2023.113901.

[29] Azzam EMS, Abd El-Salam HM, Aboad RS. Kinetic preparation and antibacterial activity of nanocrystalline poly(2-aminothiophenol). Polym Bull. 2019;76:1929–47. doi: 10.1007/S00289-018-2405-Z/FIGURES/14.

[30] Atta A, Abdeltwab E, Negm H, Al-Harbi N, Rabia M, Abdelhamied MM. Characterization and linear/non-linear optical properties of polypyrrole/NiO for optoelectronic devices. Inorg Chem Commun. 2023;152:110726. doi: 10.1016/J.INOCHE.2023.110726.

[31] Lv Y, Li P, Che Y, Hu C, Ran S, Shi P, et al. Facile Preparation and Characterization of Nanostructured BiOI microspheres with certain adsorption-photocatalytic properties. Mater Res. 2018;21:e20170705. doi: 10.1590/1980-5373-MR-2017-0705.

[32] Burton AW, Ong K, Rea T, Chan IY. On the estimation of average crystallite size of zeolites from the Scherrer equation: A critical evaluation of its application to zeolites with one-dimensional pore systems. Microporous Mesoporous Mater. 2009;117:75–90. doi: 10.1016/J.MICROMESO.2008.06.010.

[33] Lim DJ, Marks NA, Rowles MR. Universal Scherrer equation for graphene fragments. Carbon. 2020;162:475–80. doi: 10.1016/J.CARBON.2020.02.064.

[34] Haryński Ł, Olejnik A, Grochowska K, Siuzdak K. A facile method for Tauc exponent and corresponding electronic transitions determination in semiconductors directly from UV–Vis spectroscopy data. Opt Mater. 2022;127:112205. doi: 10.1016/J.OPTMAT.2022.112205.

[35] Baishya K, Ray JS, Dutta P, Das PP, Das SK. Graphene-mediated band gap engineering of WO_3 nanoparticle and a relook at Tauc equation for band gap evaluation. Appl Phys A: Mater Sci Process. 2018;124:1–6. doi: 10.1007/S00339-018-2097-0/FIGURES/5.

[36] Azizi-Toupkanloo H, Karimi-Nazarabad M, Eftekhari M, Beshkani A. Load transfer engineering via synergy of BiOI heterojunction with Ag and loading cocatalyst of $La_2O_2CO_3$ in photoelectrochemical water splitting. Int J Hydrogen Energy. 2024;57:379–87. doi: 10.1016/J.IJHYDENE.2023.12.197.

[37] Valenti M, Venugopal A, Tordera D, Jonsson MP, Biskos G, Schmidt-Ott A, et al. Hot carrier generation and extraction of plasmonic alloy nanoparticles. ACS Photonics. 2017;4:1146–52. doi: 10.1021/acsphotonics.6b01048.

[38] Brown AM, Sundararaman R, Narang P, Goddard WA, Atwater HA. Nonradiative plasmon decay and hot carrier dynamics: Effects of phonons, surfaces, and geometry. ACS Nano. 2016;10:957–66. doi: 10.1021/acsnano.5b06199.

[39] Novoselov KS, Geim AK, Morozov SV, Jiang D, Zhang Y, Dubonos SV, et al. Electric field in atomically thin carbon films. Science. 2004;306:666–9. doi: 10.1126/SCIENCE.1102896/SUPPL_FILE/NOVOSELOV.SOM.PDF.

[40] Li T, Wang B, Cao Y, Liu Z, Wang S, Zhang Q, et al. Energy-saving hydrogen production by seawater electrolysis coupling tip-enhanced electric field promoted electrocatalytic sulfion oxidation. Nat Commun. 2024;15(1):6173. doi: 10.1038/s41467-024-49931-5.

[41] Liu G, Karuturi SK, Chen H, Wang D, Ager JW, Simonov AN, et al. Enhancement of the photoelectrochemical water splitting by perovskite $BiFeO_3$ via interfacial engineering. Sol Energy. 2020;202:198–203. doi: 10.1016/j.solener.2020.03.117.

[42] Rabia M, Elsayed AM, Alnuwaiser MA. Cr_2S_3-Cr_2O_3/Poly-2-aminobenzene-1-thiol as a highly photocatalytic material for green hydrogen generation from sewage water. Micromachines. 2023;14(8):1567. doi: 10.3390/MI14081567.

[43] Helmy A, Rabia M, Shaban M, Ashraf AM, Ahmed S, Ahmed AM. Graphite/rolled graphene oxide/carbon nanotube photoelectrode

for water splitting of exhaust car solution. Int J Energy Res. 2020;44:7687–97. doi: 10.1002/er.5501.

[44] Modibane KD, Waleng NJ, Ramohlola KE, Maponya TC, Monama GR, Makgopa K, et al. Poly(3-aminobenzoic acid) decorated with cobalt zeolitic benzimidazolate framework for electrochemical production of clean hydrogen. Polymers. 2020;12:1581. doi: 10.3390/polym12071581.

[45] Naldoni A, Guler U, Wang Z, Marelli M, Malara F, Meng X, et al. Broadband hot-electron collection for solar water splitting with plasmonic titanium nitride. Adv Opt Mater. 2017;5:1601031. doi: 10.1002/adom.201601031.

[46] Ragupathi V, Raja MA, Panigrahi P, Subramaniam NG. CuO/g-C_3N_4 nanocomposite as promising photocatalyst for photoelectrochemical water splitting. Optik. 2020;208:164569. doi: 10.1016/J.IJLEO.2020.164569.

[47] Freeman E, Kumar S, Thomas SR, Pickering H, Fermin DJ, Eslava S. $PrFeO_3$ photocathodes prepared through spray pyrolysis. ChemElectroChem. 2020;7:1365–72. doi: 10.1002/celc.201902005.

[48] Huang X, Zhang M, Sun R, Long G, Liu Y, Zhao W. Enhanced hydrogen evolution from CuO_x-C/TiO_2 with multiple electron transport pathways. PLoS One. 2019;14:e0215339. doi: 10.1371/JOURNAL.PONE.0215339.

[49] Wang Z, Cao D, Wen L, Xu R, Obergfell M, Mi Y, et al. Manipulation of charge transfer and transport in plasmonic-ferroelectric hybrids for photoelectrochemical applications. Nat Commun. 2016;7:10348. doi: 10.1038/ncomms10348.